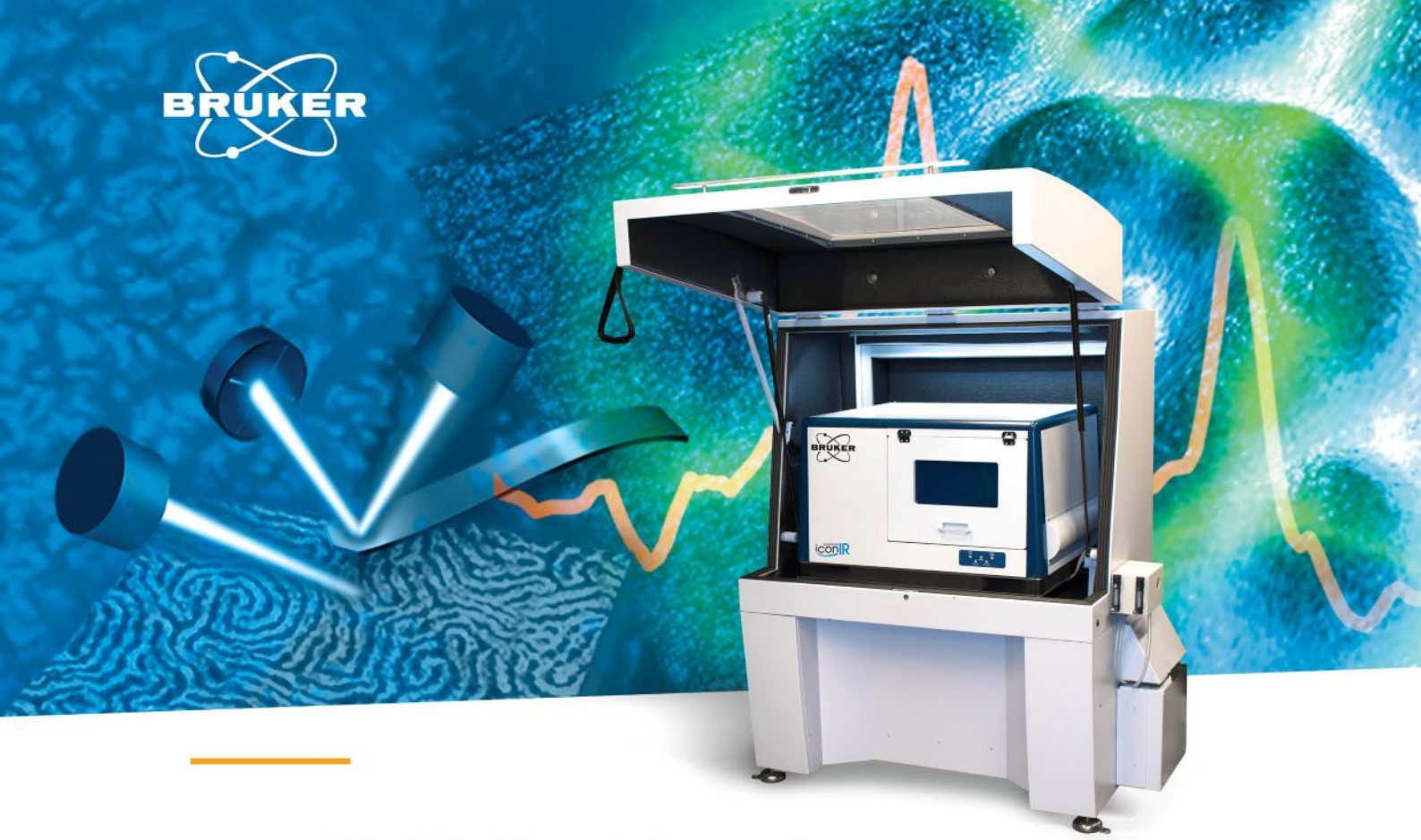

World's Most Advanced Photothermal IR Spectroscopy Solutions

Bruker's nanoscale infrared (nanoIR) spectrometers measure spatially varying physical and chemical properties in a diverse range of fields, from polymers and 2D materials to life science and micro-electronics. Fueling an impressive and growing publication record, these systems are advancing academic discovery and helping industrial companies solve critical process problems.

Proprietary spectroscopy and AFM technology:

- **NEW** Dimension IconIR large-sample system with PeakForce property mapping
- High-performance nanoIR spectroscopy with accurate and repeatable FTIR correlation
- Sub-10nm chemical resolution and monolayer sensitivity
- **NEW** Surface Sensitive AFM-IR mode with chemical probing depth to tens of nanometers

Take your materials research to the next level.
Visit www.bruker.com/nanoIR, email productinfo@bruker.com or call +1.408.376.4040/866.262.4040 for more information today.

Innovation with Integrity

Received: 14 July 2021 | Revised: 7 September 2021 | Accepted: 10 September 2021

DOI: 10.1002/pol.20210554

RESEARCH ARTICLE

JOURNAL OF POLYMER SCIENCE WILEY

Biomimetic double network hydrogels: Combining dynamic and static crosslinks to enable biofabrication and control cell-matrix interactions

Ana A. Aldana[1] | **Francis L. C. Morgan**[1] | **Sofie Houben**[2] | **Louis M. Pitet**[2] | **Lorenzo Moroni**[1] | **Matthew B. Baker**[1]

[1]Department of Complex Tissue Regeneration, MERLN Institute for Technology Inspired Regenerative Medicine, Maastricht University, Maastricht, Netherlands

[2]Advanced Functional Polymers Laboratory, Institute for Materials Research (IMO), Hasselt University, Hasselt, Belgium

Correspondence

L. M. Pitet, L. Moroni, M. B. Baker, Department of Complex Tissue Regeneration, MERLN Institute for Technology Inspired Regenerative Medicine, Maastricht University, P.O. Box 616, 6200 MD Maastricht, Netherlands.
Email: louis.pitet@uhasselt.be; l.moroni@maastrichtuniversity.nl; m.baker@maastrichtuniversity.nl

Funding information

This research has been made possible with via support of NWO (Innovation Fund Chemistry, project "DynAM" under project agreement 731.016.202), and the Dutch Ministry of Economic Affairs. Partial support (L.M.P., A.A.A., and M.B. B.) is appreciated from the Research Foundation-Flanders (FWO) under contract G080020N. S.H. is grateful for funding from a BOF-OWB mandate under contract BOF19OWB08.

Abstract

Hydrogels are promising candidates for recapitulation of the native extracellular matrix (ECM), yet recreating molecular and spatiotemporal complexity within a single network remains a challenge. Double network (DN) hydrogels are a promising step towards recapitulating the multicomponent ECM and have enhanced mechanical properties. Here, we investigate DNs based on dynamic covalent and covalent bonds to mimic the dynamicity of the ECM and enable biofabrication. We also investigate the spatiotemporal molecular attachment of a bioactive adhesive peptide within the networks. Using oxidized alginate (dynamic network, Schiff base) and polyethylene glycol diacrylate (static network, acrylate polymerization) we find an optimized procedure, where the dynamic network is formed first, followed by the static network. This initial dynamically cross-linked hydrogel imparts self-healing, injectability, and 3D printability, while the subsequent DN hydrogel improves the stability of the 3D gels and imparts toughness. Rheology and compression testing show that the toughening is due to the combination of energy dissipation (dynamic network) and elasticity (static network). Furthermore, where we place adhesive sites in the network matters; we find distinct differences when an adhesive peptide, Arg-Gly-Asp (RGD), is attached to the different networks. This DN strategy bring us closer to understanding and recreating the complex multicomponent ECM—pushing us past a materials view of cell adhesion—while enabling injectabiltiy and printing of tough hydrogels.

KEYWORDS

3D printing, biomimetic materials, double networks, dynamic covalent cross-linking, hydrogels

1 | INTRODUCTION

Well-designed extracellular matrix (ECM) mimics are needed to guide cellular behavior for effective strategies from tissue engineering to implants and wearables. The native ECM is an inherently complex and multicomponent macromolecular system that directs and responds to cellular function; recapitulating the ECM form and function remains a challenge for chemists and materials scientists. The search to recreate the complexity and function of the native ECM in tailorable and controllable polymeric systems is essential for effective control of cell–material interactions.[1] Hydrogels remain one of the most promising matrices to imitate the ECM of soft tissues due to their hydrated macromolecular network structure.[2,3] Already by using synthetically tailorable hydrogels, the effects of stiffness,[4–6] stress relaxation,[7–9] and 3D shape[10] on cell behavior and tissue formation have been elucidated; via biofabrication technologies, these hydrogels can also enable the creation of anatomically correct structures.[11]

While the majority of hydrogels used to study cell–matrix interactions and fabricate 3D tissue constructs consist of single network hydrogels, double network (DN) hydrogels are appealing candidates for recapitulating properties of the native ECM.[12,13] These DN hydrogels exhibit increased complexity, improved strength, and versatile chemical modification opportunities.[2,13] The native ECM is itself an interpenetrating network,[14,15] where different components have different functions, from the strong and static collagen I, to the dynamic rearrangement of collagen IV and laminin, to the use of glycosaminoglycans to sequester and deliver growth factors. Multicomponent and multi-network systems combined with 3D scaffold formation offer a path forward to reintroduce ECM complexity in a step-wise and rational manner.[16]

DN hydrogels combine brittle and flexible networks, typically showing superior strength compared with the corresponding individual networks.[12,13] While the brittle network helps dissipate energy via fracture of cross-links, the flexible network imparts extensibility and enables the hydrogel to recover after deformation.[17] The combination of dynamic reversible and static irreversible cross-linking make DN hydrogels appealing candidates for extrusion bioprinting applications.[18] These DN hydrogels have shown exceptional mechanics and printability, making impressive progress towards 3D biomimetic systems capable of addressing the complexity of ECM.[11–13,19]

Rational design of DN gels provides opportunities to study and control cell–matrix interactions. The vast majority of studies on synthetic and polymeric hydrogels have identified a clear link between the cell behavior and stiffness or stress-relaxation, but rely on single networks. Multicomponent networks provide unique opportunities to unravel further complexities of cell-matrix interactions. Already, tumor in vitro models based on DN hydrogels have been used investigate the role of ECM mechanics and composition on cancer cell invasion, tumorigenicity, and drug resistance.[20–22] More complex questions like the dependence of the molecular attachment of cells within a single material (adherence to one network vs the other) can also be probed.

To highlight DNs as a platform to recreate the complexity of the ECM, we set out to design a system combining both static and dynamic networks. We utilized a previously developed dynamic covalent alginate in our lab and combined with poly(ethylene glycol) diacrylate (PEGDA). Exploring the formulation space of DN formation enabled us to uncover tough hydrogels, which were cytocompatible and amenable to injection and 3D printing. Furthermore, by utilizing orthogonally reactive peptide ligation (oxime for the dynamic alginate network, thiol-ene for the static PEG acrylate network) we observed differences in cell adhesion between the networks – beginning to unravel the macromolecular complexity of cell-matrix interactions.

2 | EXPERIMENTAL SECTION

2.1 | Materials

Sodium alginate was purchased from FMC (Manugel GMB, Lot No. G9402001, ~380 kDa) and purified before use as previously reported.[23] Activated charcoal (Norit), adipic acid dihydrazide (≥98%), sodium periodate ($NaIO_4$), ethylene glycol, N-hydroxysulfosuccinimide sodium salt (≥98%, sulfo-NHS), dry poly(ethylene glycol) (PEG; MW 20.000), Irgacure 2959, triethylamine (≥99.5%, TEA), diethyl ether (≥99%) and dichloromethane (≥99.8%, DCM) were purchased from Sigma-Aldrich, without further purification. SnakeSkin™ dialysis membrane with a molecular weight cut off (MWCO) 3500 Dalton (Da), and was purchased from Thermo Fisher Scientific. Dulbecco's phosphate buffer saline (PBS, without calcium and magnesium) was purchased from ThermoFisher Scientific. Acryloyl chloride was purchased from Alfa Aesar (Ward Hill, MA). Human Dermal Fibroblasts (HDF) were purchased from ScienCell (Human Dermal Fibroblasts-adult, Catalog #2320). Dulbecco's modified Eagle's medium (DMEM, high glucose and supplemented with GlutaMAX™ and Sodium Pyruvate), DEME-F12 (low glucose), Dulbecco's phosphate buffer saline (PBS), fetal bovine serum (FBS), penicillin/streptomycin (P/S), calcein AM, ethidium homodimer, Alexa Fluor® 488 Phalloidin, DAPI and PrestoBlue™cell viability reagent were purchased from Thermo Fisher Scientific. Aminooxy RGD ([AOAC]-GGGRGDS) and cysteine-RGD (CGGGRGDS) were purchased from ChinaPeptides.

2.2 | Double network hydrogel formation

2.2.1 | Hydrogel preparation

A series of five DN formulations were evaluated. First, three stock solutions of oxidized alginate (OA) (5% w/v), PEGDA (40% w/v, 1% w/v Irgacure 2959) and adipic acid dihydrazide (ADH, 0.20 M) were prepared in PBS (13.5 mM, see 'Effect of buffer concentration' in the Supplementary Information). To prepare each solution, polymers and/or cross-linkers were weighed into 5 ml vials and dissolved in PBS solution with stirring at room temperature. Then, individual polymer solutions were mixed in different ratios to reach the final polymer concentrations as Table 1 describes. Then, ADH solution was added into the precursor solution and transferred to molds (see the Supplementary Information) to prepare dynamic cross-linked hydrogels with equimolar concentrations of aldehyde/hydrazide groups. For the characterization described in Section 2.3, samples were placed in the fridge (4 °C) for gelation overnight. For Section 2.4 and 2.5, the hydrogels were allowed to form the dynamic network overnight, then irradiated with UV light (365 nm UVP CL-1000 UV, 10 $J \cdot cm^{-2}$) for 10 min to form the second network (cross-linked PEGDA, static crosslinking). As controls, OA (2.5% w/v) and PEGDA (10%) single networks were also prepared. All hydrogel formulations are denoted OAxPy, where x and y are the weight percentage of OA and PEGDA, respectively. In addition, dynamic and static cross-linking refer to the aldehyde/hydrazide crosslinking (OA network), and the acrylate polymerization (PEGDA network), respectively.

2.2.2 | Biofunctionalization of hydrogel networks

For cell viability, DN hydrogels were biofunctionalized with aminooxy RGD (0.75 mM) via oxime ligation with aldehyde groups of OA.[23,24] Briefly, the precursor solution was prepared and RGD peptide was added immediately before the first network formation. Then, the same protocol was followed to form the dynamic and static cross-linking as Section 2.2.1 described. For cell spreading, OA2.5P10 was tested as platform to compare the effect of RGD attached to dynamic or static network on cell behavior. DN/RGD-dynamic hydrogel was obtained by coupling aminooxy RGD as described above. DN/RGD-static was obtained by thiol-ene reaction between thiol groups of cysteine-RGD and acrylate groups of PEGDA. OA2.5P10 was prepared following the previous protocol (2.2.1), with the cysteine-RGD added into the precursor solution before cross-linking. A set concentration of 0.75 mM RGD was utilized for the formation of all hydrogels.

TABLE 1 Double network hydrogel formulations

Sample	Oxidized alginate (% w/v)	PEGDA (% w/v)
OA2.5P5	2.5	5
OA2.5P10	2.5	10
OA2.5P15	2.5	15
OA2P10	2	10
OA3P10	3	10

2.3 | Characterization of DN formulations before photo-crosslinking

2.3.1 | Qualitative injectability

Hydrogels were prepared in 3 ml syringes after adding ADH and prior to photo-crosslinking, as Section 2.2.1 and SI describes. After overnight at 4 °C, hydrogels were extruded through a 22G needle by manually applying pressure to deposit a filament on a coverslip. After extrusion, we took a photo of each sample. A filament was called uniform when it was a continuous fiber (without any empty space or discontinuity along the fiber).

2.3.2 | Macroscopic self-healing

Two hydrogel discs (12 mm in diameter and 1.2 mm in thickness) of each sample were produced as described in the SI. One of each hydrogel sample was stained with CF™647 hydrazide solution (0.67 mM, blue, Sigma Aldrich). All the hydrogels were cut in two pieces with a scalpel and then two different colored pieces were placed in contact for 24 h at 4 °C. Then hydrogel healing was checked by manual stretching with tweezers. For testing the self-healing property of DN hydrogels, the same protocol was followed with the exception that gels were cured (10 min, 365 nm) before staining with the CF647 dye.

2.3.3 | Printability

All precursor-DN formulations were prepared into a 3 ml syringe with stoppers and stored in the fridge overnight. To investigate printability, continuous filament (zigzag path, 10 mm in width and 32 mm in length), 3-layer hollow cube (10 mm in width and length and 2 mm in

height) and grid-like structures (two layers 10 × 10 grid, 15 mm in width and length) were fabricated using the extrusion-based BioX bioprinter (CellInk, Sweden). Conical plastic needles (VIEWEG GmbH, Germany) were fixed to the syringes with an inner diameter of 22 G (0.41 mm). The pressure applied to form a continuous filament depends on the hydrogel formulation, which was lowest, 20 kPa, for the formulation with the lowest solids (OA2.5P5) and highest, 200 kPa, for the formulation with the highest solids (OA3P10). All hydrogels had one drop of food coloring dye (red) added during the mixing process for better post-print visualization.

2.4 | Mechanical properties of DN hydrogels

2.4.1 | Rheology

Rheological measurements were performed using a DHR-2 from TA instruments equipped with an 8 mm sand-blasted parallel plate geometry. For UV measurements, a quartz bottom plate and UV-Light attachment with a liquid light guide connected to an M365LP1 Mid Power Mounted LED at 365 nm from Thorlabs was used. A DC2200 1 Channel LED Driver (10A) was used to control the LED intensity at the sample interface. The light intensity was calibrating using the fitted sensor provided by TA instruments – circular with a close fit over the lower geometry to capture the true light intensity received by the sample. A current of 1400 mA was used, which corresponds to a light intensity of 78 $mW \cdot cm^{-2}$. Once the preformed hydrogel discs were loaded onto the rheometer, the upper geometry was lowered until an axial force of 0.01 N was achieved. Time sweeps were performed for 5 min at 23 °C (measured RT) with a frequency of 0.5 Hz and a strain of 1% to obtain a baseline reading for each sample. A second 300 s time sweep was immediately initiated after, during which the sample was irradiated with 365 nm light from 60–300 s to monitor cross-linking.

2.4.2 | Compression testing

Compression testing was performed on a Shimadzu AGS-X mechanical tester equipped with a 500 N load cell at room temperature. Gels were compressed at a speed of 1 mm/min until a strain of 80% was reached. The stress is recorded as the load applied divided by the area of the sample in original state. The strain is recorded as the displacement of the compression plates divided by the starting distance between the compression plates. The elastic modulus (E) was calculated as the slope of the stress–strain curve for a strain below 25%.

2.5 | Cells and DN hydrogels

Human dermal fibroblasts (HDF) were cultured in Dulbecco's modified Eagle's medium (DMEM, high glucose) supplemented with GlutaMAX™, Sodium Pyruvate, 10% (v/v) fetal bovine serum (FBS) and 1% (v/v) P/S. Cells were passaged at 80%–85% confluence and were used after passage 11 for cell experiments.

Hydrogel solutions were prepared as Section 2.2 described and transferred to a flat bottom black 96-well plate. Then, DN hydrogels were washed with DMEM (twice, 5 min each) to equilibrate with cell culture medium. HDF cells were seeded on top of the hydrogels at a density of 50,000 cells/well. Controls were prepared on the same tissue culture plate (TCP) with 25,000 cells/well. Live/Dead and DAPI/Phalloidin assays were carried out to evaluate cell viability and morphology, respectively (see the Supplementary Information).

3 | RESULTS AND DISCUSSION

3.1 | Polymer synthesis

In order to realize our design of DN hydrogels, we first needed to create the individual polymer systems. The DN hydrogels were prepared by combining hydrazone cross-linked OA and poly(ethylene glycol)-diacrylate (PEGDA) to form the dynamic and static networks, respectively (Figure 1). These polymers are biocompatible and widely studied for tissue engineering applications.[25–27] First, the oxidation of alginate was carried out using sodium periodate ($NaIO_4$) (see the Supplementary Information), as previously reported. The oxidation of alginate (theoretical 10% degree of oxidation) was confirmed qualitatively by ^{1}H-NMR spectroscopy (Figure S1). PEGDA was synthesized by acrylation of the terminal hydroxyls groups of PEG ($M_n = 20$ kg mol^{-1}) with acryloyl cholride to enable photo cross-linking (see the Supplementary Information). The acrylation of PEG was characterized by ^{1}H-NMR spectroscopy and GPC as described in the Supplementary Information (Figure S2).

3.2 | Double network hydrogel optimization

After preparing OA and PEGDA, a series of hydrogel formulations were prepared to determine the optimal

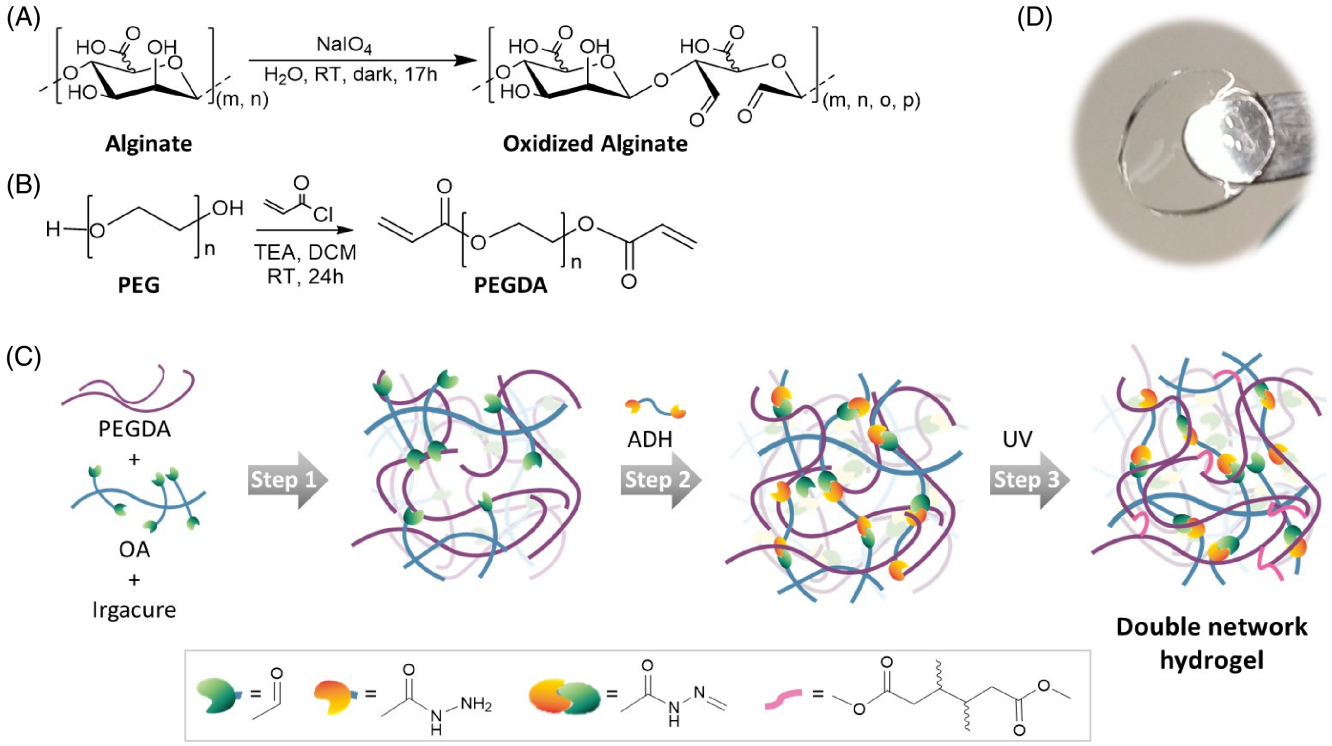

FIGURE 1 Creating double network hydrogels based on dynamic and static cross-linking chemistries. (A) Synthesis of oxidized alginate; (B) synthesis of PEGDA; (C) scheme of double network formation; (D) image of DN hydrogel

window of DN formation. These formulations are denoted OAxPy, where x and y are the weight percentage of OA and PEGDA, respectively. For example, a hydrogel with 2 wt% OA and 10 wt% PEGDA is described as OA2P10.

First, we explored the method of DN hydrogel formation. After a few trials, we found that a three-step process produced good results: (1) The OA, PEGDA, and Irgacure (photo-initiator) are mixed in precursor solution, (2) The dynamic covalent network is formed first via the addition of adipic acid dihydrazine (ADH) and mixing, (3) The covalent network is formed via UV irradiation. Initially, we observed a strong effect of salt concentration on the mixing/demixing of the two networks upon the first cross-linking (see Effect of PBS concentration and Figure S3b). In the first attempt, the preparation of precursor solutions in the commercial PBS led to phase separation of the precursor-DN formulations after adding ADH. This issue was resolved by using lower concentrations of PBS for the initial DN formation.

The adipic acid dihydrizide (ADH) was added to the precursor solution to form the dynamic network. Aldehyde groups along the OA and hydrazide groups of ADH react quickly via Schiff base condensation to form hydrazone bonds (cross-links). Upon formation of the hydrazone bonds, the polymer solutions became transparent homogenous gels for all DN formulations. The dynamic nature of these reversible bonds was investigated by assessing the viscoelasticity and self-healing properties (see Section 3.2). Dynamic hydrogels allow cells to rearrange their environment (by breaking and reforming the bonds), showing promising applications in cell culture platforms and 3D bioprinting.[18,28,29]

In the second step, the dynamic covalent cross-linked hydrogels were exposed to UV light (365 nm). The photo-cross-linking of acrylate end groups of PEGDA took place in the presence of Irgacure (initiator) to create covalent cross-links, generating a static network. After UV irradiation, all hydrogels were observed to be macroscopically stiffer, which increased with PEGDA concentration. While the viscoelasticity of dynamic and reversibly cross-linked hydrogels plays a key role on cell spreading, migration, and communication, their timescale dependent properties (e.g., theoretical infinite swelling capacity) can affect long-term use in cell culture medium.[18,28] The second network allows DN hydrogels to be stable in PBS solution (Figure S3b), showing potential applications in long-term culture.

3.3 | Qualitative injectability, self-healing, and printability

The dynamic covalent crosslinking of the first network dominates the behavior of the precursor-DN hydrogels

before UV irradiation and covalent fixation. Since single networks of dynamically cross-linked alginate have shown good injectability and printability,[18] we wanted to investigate these dual network formulations when only the dynamic network is formed. Defining qualitative injectabilty as facile extrusion by hand,[30] the precursor-DN hydrogel formulations (without UV irradiation) were manually extruded through the syringe. All formulations were injectable through the 22G needle via simple manual application of force. (Figure S4). We observed that the overall polymer concentration had the most profound effects on injectability with higher polymer concentration requiring more pressure. Several of the formulations were able to form a uniform fiber after extrusion through the syringe/needle. OA 2.5 wt% with PEGDA 10 wt% (OA2.5P10, Figure 2A) showed the best balance between the following parameters: filament formation, applied pressure, and nozzle diameter, which are critical for injection and bioprinting applications. The dynamic nature of the hydrazone bonds leads to shear-thinning behavior, viscous flow under shear stress, and recovery when the applied stress is removed due to the self-healing capability. This behavior dominates even in the presence of another polymer (i.e., PEGDA).

We previously reported that the dynamic cross-linking of OA with adipic acid dihydrazide exhibits self-healing properties,[23] wherein the influence of a second static network was investigated. Macroscopic self-healing of the hydrogels was tested (Figure 2B). All precursor-DN hydrogel formulations (i.e., before covalent cross-linking) were able to heal even at high concentration of PEGDA, corroborating that the dynamic nature of the first network dominates before UV cross-linking. The blue dye is a high molecular weight compound (≈ 3 kg mol^{-1}) with hydrazide groups, which reacts with aldehyde groups of the OA network. Each hydrogel was completely blue after 24 h, corroborating the dynamics and reversibility of this hydrazone linkage under the conditions explored (Figure 2B). To further analyze the self-healing and injectability, we carried out a shear rheometry testing of the OA2.5P10 formulation. The clear shear dependent viscosity and cyclic recovery after high applied shear (Figure S5) also corroborate the dynamicity of the hydrazone cross-links. Within the fully formed DN hydrogels (after UV crosslinking), the OA2.5P15 hydrogel was also able to self-heal, while the formulations with less PEGDA (5% and 10%) were not. Even though the hydrazone dye remained mobile in these 5 and 10% PEGDA formulations, only the higher concentrations maintained self-healing.

These shear-thinning and self-healing hydrogels are promising not only for injectability, but also for 3D bioprinting. As mentioned above, all hydrogels were extruded easily through a needle, forming intact fibers. We then tested them as biomaterial inks for extrusion-based 3D printing (Figure 2C). The OA2.5P10, OA3P10, and OA2.5P15 hydrogels showed similar printability in term of homogenous and defined structures (Figure S6) at a nozzle diameter of 22G. The printed structures with precursor-DN formulations at high-polymer concentration (OA2P15) maintained their shape, while the hydrogels with lower concentration of polymers collapsed shortly after printing (Figure S6).

3.4 | Mechanical characterization

3.4.1 | Rheology

As a singular network, OA with hydrazone crosslinks possesses significant viscoelastic behavior.[23] Here, the

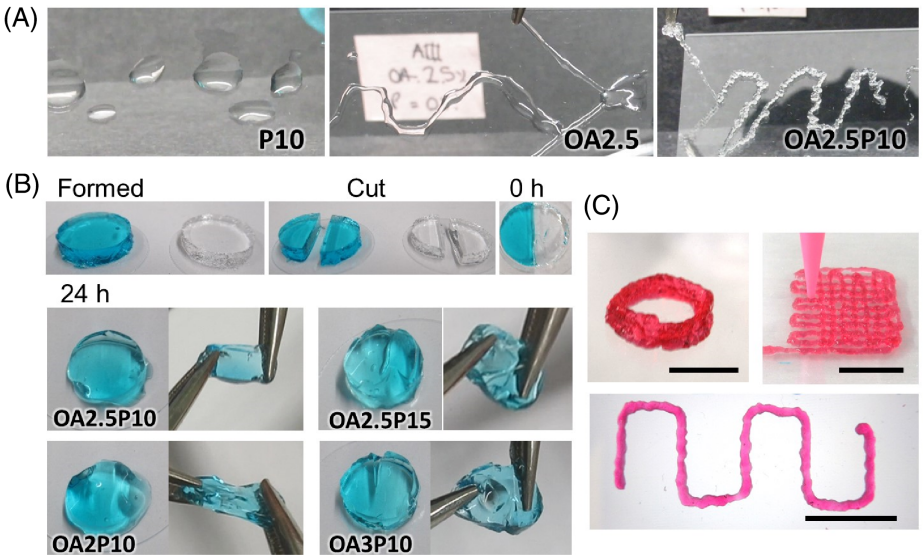

FIGURE 2 The dynamic network allows precursor-DN formulations to have shear-thinning and self-healing properties. (A) Images of filaments extruded through syringe with 22G needle; (B) Macroscopic self-healing test, where one of gel was colored with blue dye (CF647 hydrazide), cut in half, left to heal, and tested at 24 h; (C) Extrusion 3D printed OA2.5P15 hydrogel structures, scale bar 10 mm

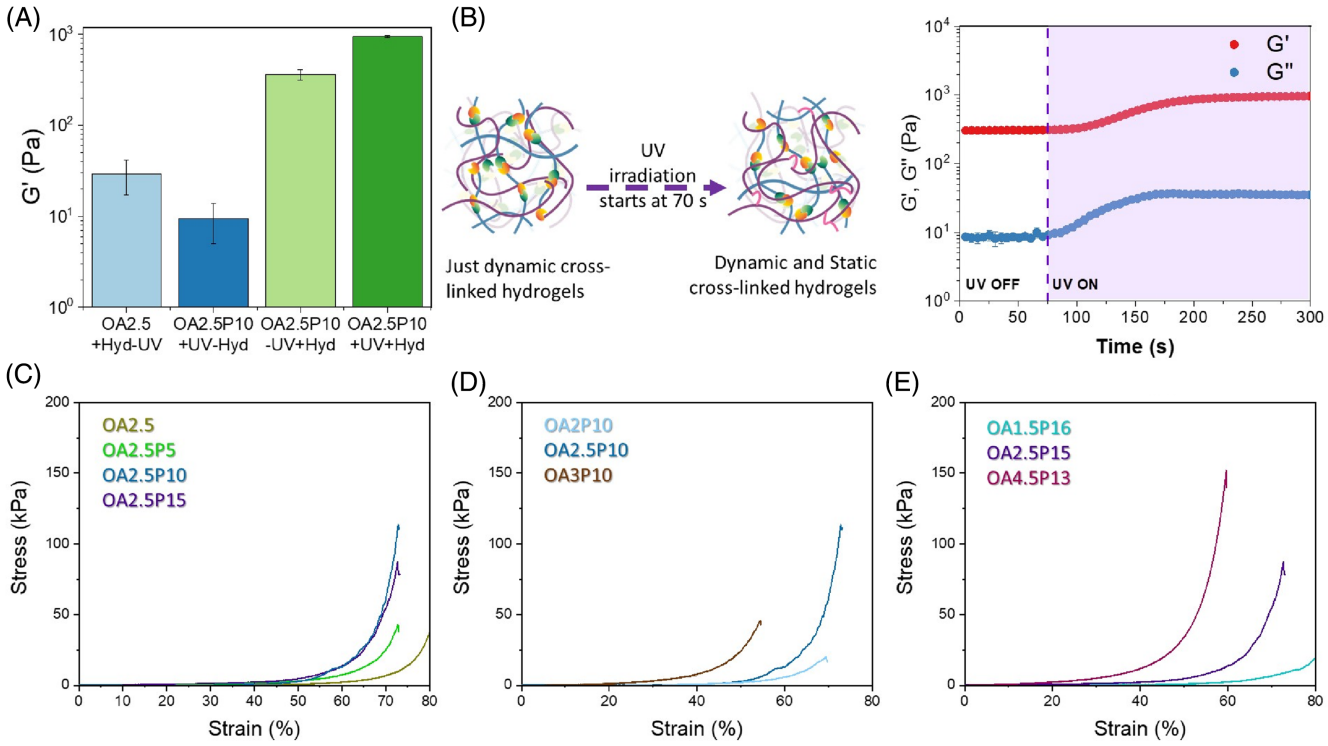

FIGURE 3 Both dynamic and static networks contribute to the toughening of DN hydrogels. Rheology: (A) Storage modulus of DN and single network formulations comparing both crosslinkings; (B) Dynamic moduli (G', G") as a function of time for OA2.5P10 at a constant 77 mW cm^{-2} intensity. Uniaxial compression testing: Stress–strain curves of (C) The OA2.5Py, (D) OAxP10, and (E) OA_xP (x + y = 17.5) hydrogels series

role of the static cross-linking in the overall mechanical properties of DN hydrogels was investigated by rheology (Figure 3A, B).

The storage modulus of all hydrogels were measured and compared in Figure 3A. Considering first the dynamic cross-linked OA network (OA2.5), we measured an initial shear modulus of 29 ± 12 Pa. The addition of PEGDA (not cross-linked), bringing the total polymer content to 12.5 wt%, led to the formation of hydrazone cross-linked OA2.5P10 hydrogels with a shear modulus of 363 ± 48 Pa. Interestingly, the same composition when cross-linked with only the PEGDA network in the absence of hydrazone yielded very soft hydrogels with a G' of 9 ± 4 Pa. This highlights the difference in available cross-linking sites between a side-chain functionalized versus telechelic (i.e., PEGDA) polymer. Despite possessing four times as much polymer, the PEGDA network has a much lower cross-link density, giving rise to extremely soft hydrogels. This also evidences the significant role of the dynamic crosslinking on the DN hydrogel mechanics. Upon irradiation with 365 nm light (Figure 3B), the storage modulus increased 3-fold to 947 ± 30 Pa over the course of 3 min, indicating the successful light-mediated cross-linking of the PEGDA. Notably, the shear modulus of the DN is far greater than the sum of its parts, compared to the singly cross-linked hydrazone and PEGDA networks possessing shear moduli of 363 and 9 Pa, respectively.

On a macroscopic scale, the DN hydrogels were much stickier while handling compared to OA2.5 hydrogel, suggesting the PEGDA influences their behavior. Following UV treatment, the resulting DN hydrogels were noticeably more rigid while handling, but still sticky upon the initial addition of 10 wt% PEGDA.

3.4.2 | Compression testing

Uniaxial compression testing was performed to determine the mechanical properties and their relationship with the DN compositions. The different compositions of DN hydrogels were divided in three series: OA2.5Py, varying the amount of PEGDA; OAxP10, varying the amount of OA; OAxPy, keeping the total polymer concentration constant. Hydrogels in the series OA2.5Py (with 2.5 wt% of OA) exhibited similar values of fracture strain independently of PEGDA concentration, while OA single network hydrogel can resist up to 80% compression without fracture (Figure 3C and Table 2). The photo-cross-linked network improved the compressive strength

TABLE 2 Mechanical properties of double network hydrogels determined by uniaxial compression testing

Sample	Elastic modulus (kPa)	Compressive strength (kPa)	Maximum strain (%)
OA2.5	1.2 ± 0.2	37.2 ± 6.1	N.A.
OA2.5P5	4.1 ± 0.6	41.8 ± 6.1	72.8 ± 5.3
OA2.5P10	0.8 ± 0.7	113 ± 16	72.8 ± 6.0
OA2.5P15	4.1 ± 1.1	87 ± 11	72.7 ± 9.8
OA2P10	2.8 ± 1.2	19.3 ± 4.2	69.6 ± 7.5
OA3P10	13.6 ± 4.8	44.4 ± 9.6	54.3 ± 4.5
OA1.5P16	3.5 ± 0.5	19.0 ± 2.7	N.A.
OA4.5P13	20.2 ± 4.2	153 ± 21	59.8 ± 6.2

of DN hydrogels compared to OA2.5 hydrogel. Notably, 10 wt% of PEGDA reached the highest compressive strength (113 kPa) in this series. The highest OA concentration (3 wt%) in OAxP10 hydrogels showed the highest elastic modulus (13.6 kPa) and the lowest fracture strain (54.3%) in this series (Figure 3D and Table 2). The highest concentration of either PEGDA or OA network in both series exhibited the lowest mechanical strength. This behavior could be associated with differing homogeneity between the hydrogels or a different effect of total polymer concentration and the DN composition on hydrogel mechanics.

Therefore, we compared a series of OAxPy hydrogels with same polymer concentration ($x + y = 17.5$ wt%) to gain further insight into the underlying mechanism of the interaction forces on the DN and the corresponding impact on the mechanical properties (Figure 3E and Table 2). The stress–strain curves of this series clearly indicate that the OA and PEGDA network affects the mechanical properties independently from the polymer concentration. Elastic modulus and compressive strength increase while maximum strain decrease with increasing OA network content (dynamic cross-linking) with respect to PEGDA network (static cross-linking). Considering the cross-linking degree is determined by the aldehyde and acrylate groups in the OA and PEGDA networks, respectively, the DN hydrogel with higher dynamic cross-linking than static one (OA4.5P13, $ratio_{dynamic/static} = 1.9$) enhanced the mechanical strength and lowered maximum strain before fracture (Table S1). On the other hand, predominant static cross-linking (OA1.5P15, $ratio_{dynamic/static} = 0.5$) leads to higher extensions. These results suggest that the dynamic cross-linking can dissipate mechanical energy supporting higher compression stress, while the static cross-linking allow for improved elasticity. Zhao and co-workers reported a DN hydrogel system based on PEGDA and alginate.[27] They found similar mechanical behavior, concluding that the dynamic ionic cross-linking within the alginate network dissipates mechanical energy and the covalent crosslinking from the PEGDA network maintains elasticity under large deformations. They also showed that PEGDA based on long chains (20 $kg \cdot mol^{-1}$) allow for higher stretchability of DN hydrogels. Zhou and co-workers explored DN hydrogels by combining oxidized dextran and gelatin methacrylate to form a dynamic and static network, respectively.[31] They also corroborated that the toughening observed on DN hydrogels results of the combined mechanism of mechanical energy dissipation and high elasticity conferred by dynamic and static covalent cross-linked networks, respectively.

3.5 | Cell culture on DNs hydrogels

The combination of dynamic and static networks allow us to develop hydrogels promising for regenerative medicine. The balance between strength and viscoelasticity plays a key role in intercellular communication and

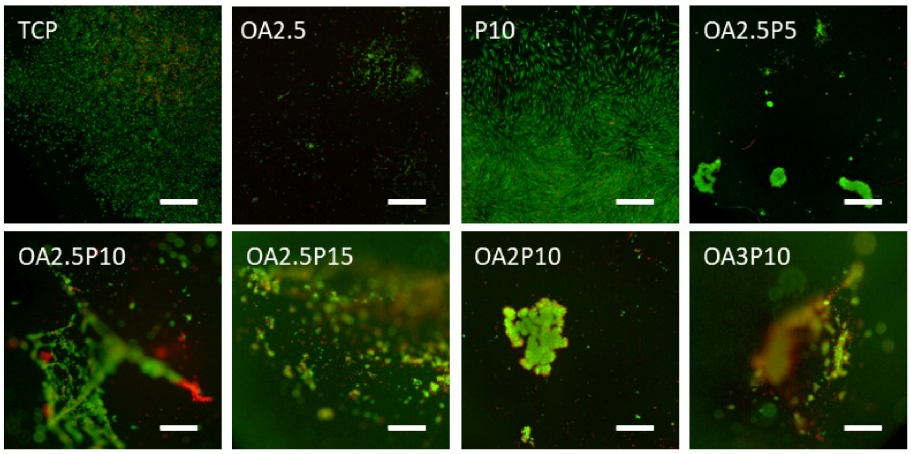

FIGURE 4 Fibroblasts seeded on DN hydrogels show high cell viability. Images of HDF cells stained with calcein-AM (green, live) or ethidium homodimer (red, dead) after 3 days on SN (single network hydrogel), DN (double network hydrogel) and TCP (tissue culture plate, control). Scale bar: 500 μm

functional tissue repair. Therefore, the basic cytocompatibility and formation process of these gels were explored. Human dermal fibroblasts (HDFs) were seeded on top of SN and DN hydrogels for 24 h and 72 h (Figure S7 and Figure 4, respectively). As PEG and alginate lack any intrinsic cell adhesion ligands, we chose to leverage the oxime ligation and incorporate aminooxy-modified RGD peptide to allow HDF-matrix interactions through integrin binding. Staining and live/dead analysis are consistent with high cell viability (alive, green; red, dead) in all hydrogels after 3 days (Figure 4). Furthermore, the cells were able to migrate into the DN hydrogels, being noticeably tridimensional on the OA2.5P10, OA2.5P15, and OA3P10 hydrogels. Lower amount of cells were observed in and on the OA2.5P5 and OA2P10 hydrogels, which was attributed to their faster swelling and erosion over the course of the experiment. The high cell viability and migration, as the DN hydrogels showed, are key criteria for tissue maturation in future applications.

While high cell viability and some migration was observed, we also noted that cell spreading and rearrangement were superior in OA2.5P10 (see OA2.5P10 in Figure 4). Jeong and co-workers have shown that mechanical stiffness of collagen hydrogels (elastic modulus of 0.7, 1.6, and 2.2 kPa) can act as a signal to regulate cell behavior.[32] Increasing modulus was concomitant with decreased cellular spreading, nuclear aspect ratio, and growth rate. Interestingly, OA2.5P10 hydrogel shows an elastic modulus (see Section 3.3) similar to their softer hydrogel (0.7 kPa), which supported cell spreading and proliferation.

Cell morphology and density on all hydrogels clearly depended on the hydrogel formulation, and consequently their mechanical properties and cross-linking degree. Soft hydrogels (OA2.5P10) allowed cells spread and migrate, but hydrogels with low cross-linking (OA2.5P5 and OA2P10) eroded during culture and staining, decreasing cell density. On the other hand, cells kept a rounded morphology in stiff hydrogels (OA3P10 and OA2.5P15).

Since the relationship between hydrogel stiffness and cell spreading, differentiation, and proliferation has been investigated widely,[7,33,34] here we explored these DN hydrogels from a molecular perspective. These DN hydrogels provide a unique opportunity to investigate and decouple bulk mechanical properties from the molecular networks to which cells could attach. For example, within a hydrogel with a set of mechanical properties, does a cell sense the properties of the bulk materials or of the molecular environment to which it attaches? Therefore, we explored if cells are capable of sensing the RGD ligands attached to dynamic or static networks, using one formulation.

Conveniently, RGD can be ligated to the different networks via orthogonal, click-type reactions: oxime ligation for dynamic network, and thiol-ene for the static network. RGD peptide (0.75 mM) was attached to OA or PEGDA backbone of the OA2.5P10 hydrogel, to form the DN/RGD-dynamic and DN/RGD-static hydrogels, respectively. Hydrogels were explored with HDFs, a commonly used model for cell adhesion, over the course of 7 days. For visualizing the cellular morphology on these hydrogels, F-Actin (green, cytoskeletal organization) and nuclei (blue) were stained at day 1, 3, and 7 (Figure 5A). Cells adhered and spread in both DN/RGD-dynamic and DN/RGD-static hydrogels; however, their temporal profiles and morphology showed differences. The fluorescent micrographs showed that cells spread quickly in the DN/RGD-dynamic hydrogel, but fewer and rounded cells were seen over time comparing with the RGD-static one. On the other hand, cells spread slowly in the DN/RGD-static hydrogel, yet the spindle-like morphology of cells became more elongated and thinner by day 7.

To further evaluate the role of the molecular network on cells, cell morphometric parameters (Figure 5B–D) were determined using image analysis. Analyzing the area of cells (Figure 5B) revealed that the mean area was affected significantly by the hydrogel at day 1 and 7. Higher cell areas were seen at day 7 compared to day 1 and 3 in DN/RGD-dynamic hydrogels, while cell areas clearly increase their area in DN/RGD-static, indicating different cell spreading depending on the molecular network approach. When looking at the spread of the data, the dynamic networks show more skew towards highly spread cells in early timepoints, while the static networks approach exhibit a gradually cell spreading over time.

In order to analyze the difference in cell morphology, we also compared the cell circularity for both samples over time. As Figure 5C shows, the circularity of cells in RGD-dynamic samples rapidly decreased by day 1 and kept their shape (moderate circularity) over time, while cells in RGD-static samples showed a significant decrease of mean circularity (more polygonal in shape) over time. Furthermore, the statistical analysis of circularity comparing DN/RGD-static and DN/RGD-dynamic at same days also suggests that the molecular network influences cell shape. To gain further insight into cell morphology, the aspect ratio was analyzed as a measure of cell elongation (Figure 5D). In DN/RGD-dynamic hydrogel, cells maintained a similar average extent of elongation over time. The RGD-static hydrogel showed an increase of the mean aspect ratio of cells towards a more spindle-like morphology. When looking at the distribution of the data, the dynamic networks have more outlier highly spread cells at the early timepoints, which then decreases, while the static networks consistently provide a more normal distribution with increasing aspect ratio over time.

The quantitative analysis of cell morphology in our DN hydrogels clearly showed that the molecular

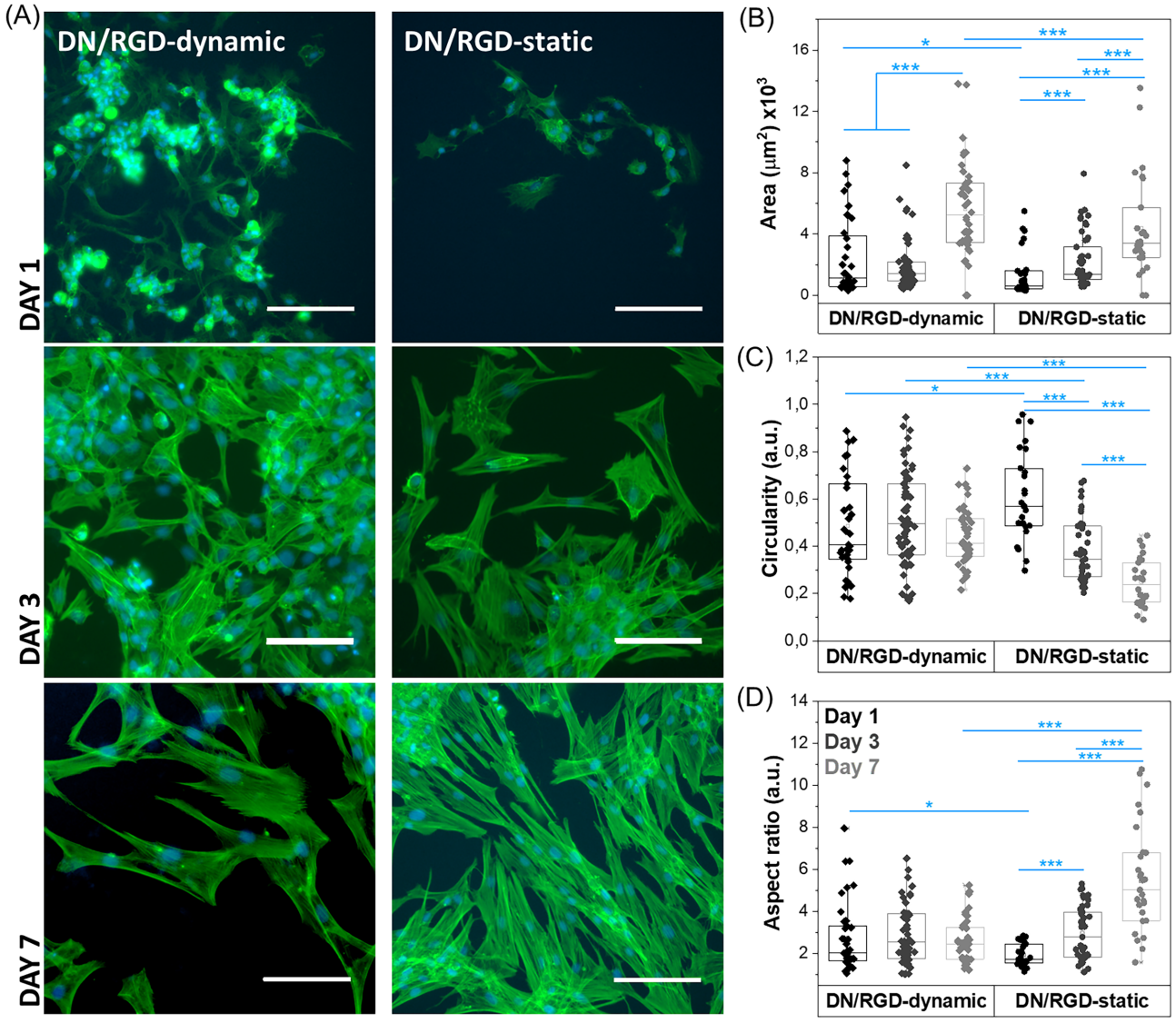

FIGURE 5 The molecular site of RGD attachment plays a significant role on HDF cells. (A) Images of HDF cells stained with Phalloidin (green, F-actin) and DAPI (blue, nuclei) after 1, 3, and 7 days on DN/RGD-dynamic (OA2.5 P10 DN hydrogel with RGD attached to OA network) and DN/RGD-static (OA2.5 P10 DN hydrogel with RGD attached to PEGDA network). Scale bar: 100 μm. Analysis of cell morphometric parameters: (B) Area, (D) Circularity ($C = 4\pi \cdot \text{area} \cdot \text{perimeter}^{-2}$, 1 = circle) and (D) Aspect ratio were analyzed at day 1, 3, and 7 for HDFs on DN/RGD-dynamic and DN/RG-static ($N_{cells} \geq 35$; $N_{experiments} \geq 2$). Statistical significance was determined by the Mann–Whitney test (*$p < 0.05$, ***$p < 0.001$). Statistical significance given compares same sample at different days and same day different samples

environment of RGD ligands affects the cell spreading of HDFs. The attachment of RGD peptide to dynamic network drives a few of the cells in a population to spread quickly and decrease the cell density over time. In contrast, RGD immobilization in the static network decreases cell spreading rate and increases cell elongation. We hypothesized that this difference in cell behavior is due to: (1) Dynamic nature of OA network allowed cells to move and reorganize for active RGD clustering and integrin activation, but did not allow sufficient force buildup, and (2) Static nature of PEGDA network kept the availability of RGD ligands over time allowing force buildup.

Recently, Yang and co-workers reported the effect of the lifetime of host-guest supramolecular cross-linking of hyaluronic acid hydrogels on hMSC spreading within a single network multi-component hydrogel.[35] They found that conjugating the RGD ligands to hyaluronic acid (HA) polymers with a more dynamic crosslink (i.e., shorter lifetime) attachment led to hMSC cells spreading faster than RGD connected to HA polymers with less dynamic crosslinks (i.e., longer lifetime). Furthermore, they compared the static (covalent bond) and dynamic (host-guest) conjugation of RGD to the same network. In their study, cells did not spread in the

supramolecular-RGD hydrogels (the assay was carried out during only 3 days). They conclude that the supramolecular conjugation of RGD to network was not persistent enough to support cell spreading. In our work, we evaluated the effect of the dynamics of networks via RGD conjugation to different networks in a DN hydrogel (either dynamic or static cross-linking). This allowed us to interrogate the role of distinct and individual molecular networks on cell spreading. Interestingly, both studies found a definitive benefit to the kinetics of cell spreading when RGD is attached to more mobile polymers within a network or within a more dynamic network; this alignment of results across experimental design may imply a significant role on network dynamics on the speed of cellular adhesion.

Jonkheijm and co-workers have explored cucurbit[8]uril (CB^8)-based host-guest systems to display RGD ligands and compared with static surfaces where RGD were covalent immobilized. They found that even though the dynamic interactions and covalent bonds involve different forces at molecular level, cell adhesion strengths were not significant difference between these surfaces.[36] They also developed an electrical-responsive CB[8]-based host-guest system, where RGD ligands release by applying a suitable electrical potential.[37] The decrease of ligand presentation affected more than 90% of the cells became rounded and detached.

4 | CONCLUSIONS

We successfully created DNs based on biocompatible polymers combining two cross-linking chemistries: dynamic covalent imine formation and static covalent acrylate polymerization. Both dynamic and static elements allow for tough hydrogels with enhanced mechanical properties. The formation of the dynamic network allowed for self-healing and injectability attributes, while the static network allowed improved stability on cell culture conditions. The synergetic effect of both networks makes these DN hydrogels tough and led to injectibility and 3D printing.

The developed DN hydrogels were also a great platform to study the role of the molecular environment on cell behavior. We observed that the molecular site of RGD attachment plays a significant role on the adhesion of HDF cells. Fibroblasts spreading, in terms of rate and elongation, was significantly different depending their interactions with the molecular network within the same DN material.

The rational design of these DNs allow us to move forward towards more spatiotemporally complex materials, which could recreate the dynamic and complex multicomponent ECM. This work not only highlights the potential of DN hydrogels as biomimetic ECM materials, but also draws attention to potential intricacies in cell-matrix interactions, which are not possible with single network hydrogels.

ACKNOWLEDGMENTS

This research has been made possible with via support of NWO (Innovation Fund Chemistry, project "DynAM" under project agreement 731.016.202), and the Dutch Ministry of Economic Affairs. Partial support (L. M. Pitet, A. A. Aldana, and M. B. Baker) is appreciated from the Research Foundation-Flanders (FWO) under contract G080020N. S.H. is grateful for funding from a BOF-OWB mandate under contract BOF19OWB08.

DATA AVAILABILITY STATEMENT

Data from this study is available upon request from the authors.

ORCID

Ana A. Aldana https://orcid.org/0000-0003-4997-7982
Matthew B. Baker https://orcid.org/0000-0003-1731-3858

REFERENCES

[1] A. Khademhosseini, R. Langer, *Nat. Protoc.* **2016**, *11*, 1775.
[2] A. P. Dhand, J. H. Galarraga, J. A. Burdick, *Trends Biotechnol.* **2021**, *39*, 519.
[3] S. C. Neves, L. Moroni, C. C. Barrias, P. L. Granja, *Trends Biotechnol.* **2020**, *38*, 292.
[4] A. J. Engler, S. Sen, H. L. Sweeney, D. E. Discher, *Cell* **2006**, *126*, 677.
[5] B. Bachmann, S. Spitz, B. Schadl, A. H. Teuschl, H. Redl, S. Nurnberger, P. Ertl, *Front Bioeng. Biotechnol.* **2020**, *8*, 373.
[6] D. E. Discher, P. Janmey, Y.-l. Wang, *Science* **2005**, *310*, 1139.
[7] O. Chaudhuri, L. Gu, D. Klumpers, M. Darnell, S. A. Bencherif, J. C. Weaver, N. Huebsch, H.-p. Lee, E. Lippens, G. N. Duda, D. J. Mooney, *Nat. Mater.* **2016**, *15*, 326.
[8] O. Chaudhuri, L. Gu, M. Darnell, D. Klumpers, S. A. Bencherif, J. C. Weaver, N. Huebsch, D. J. Mooney, *Nat. Commun.* **2015**, *6*, 6365.
[9] S. Tang, H. Ma, H.-C. Tu, H.-R. Wang, P.-C. Lin, K. S. Anseth, *Adv. Sci.* **2018**, *5*, 1800638.
[10] K. Metavarayuth, P. Sitasuwan, X. Zhao, Y. Lin, Q. Wang, *ACS Biomater. Sci. Eng.* **2016**, *2*, 142.
[11] C. Mota, S. Camarero-Espinosa, M. B. Baker, P. Wieringa, L. Moroni, *Chem. Rev.* **2020**, *120*, 10547.
[12] Z. Gu, K. Huang, Y. Luo, L. Zhang, T. Kuang, Z. Chen, G. Liao, *Wiley Interdiscip. Rev. Nanomed. Nanobiotechnol.* **2018**, *10*, e1520.
[13] A. A. Aldana, S. Houben, L. Moroni, M. B. Baker, L. M. Pitet, *ACS Biomater. Sci. Eng.* **2021**, *7*, 4077.
[14] W. P. Daley, S. B. Peters, M. Larsen, *J. Cell Sci.* **2008**, *121*, 255.
[15] F. Gattazzo, A. Urciuolo, P. Bonaldo, *Biochim. et Biophys. Acta (BBA) - General Sub.* **2014**, *1840*, 2506.
[16] H. W. Ooi, S. Hafeez, C. A. van Blitterswijk, L. Moroni, M. B. Baker, *Mater. Horiz.* **2017**, *4*, 1020.
[17] T. Nonoyama, J. P. Gong, *Proc. Ins. Mech. Eng. H.* **2015**, *229*, 853.

[18] F. L. C. Morgan, L. Moroni, M. B. Baker, *Adv. Health. Mater.* **2020**, *9*, e1901798.
[19] L. Moroni, J. A. Burdick, C. Highley, S. J. Lee, Y. Morimoto, S. Takeuchi, J. J. Yoo, *Nat. Rev. Mater.* **2018**, *3*, 21.
[20] A. J. Berger, K. M. Linsmeier, P. K. Kreeger, K. S. Masters, *Biomaterials* **2017**, *141*, 125.
[21] W. Xu, J. Qian, Y. Zhang, A. Suo, N. Cui, J. Wang, Y. Yao, H. Wang, *Acta Biomater.* **2016**, *33*, 131.
[22] H.-Y. Liu, M. Korc, C.-C. Lin, *Biomaterials* **2018**, *160*, 24.
[23] S. Hafeez, H. W. Ooi, F. L. C. Morgan, C. Mota, M. Dettin, C. Van Blitterswijk, L. Moroni, M. B. Baker, *Gels* **2018**, *4*, 4.
[24] A. Zamuner, M. Cavo, S. Scaglione, G. M. Messina, T. Russo, A. Gloria, G. Marletta, M. Dettin, *Materials* **2016**, *9*, 9.
[25] B. Sarker, A. R. Boccaccini, in *In Alginates and Their Biomedical Applications* (Eds: B. H. A. Rehm, M. F. Moradali), Springer Singapore, Singapore **2018**, p. 121.
[26] M. B. Browning, S. N. Cereceres, P. T. Luong, E. M. Cosgriff-Hernandez, *J. Biomed. Mater. Res. Part A* **2014**, *102*, 4244.
[27] S. Hong, D. Sycks, H. F. Chan, S. Lin, G. P. Lopez, F. Guilak, K. W. Leong, X. Zhao, *Adv. Mater.* **2015**, *27*, 4035.
[28] A. M. Rosales, S. L. Vega, F. W. DelRio, J. A. Burdick, K. S. Anseth, *Angew. Chem. Int. Ed. Engl.* **2017**, *56*, 12132.
[29] S. Uman, A. Dhand, J. A. Burdick, *J. Appl. Polym. Sci.* **2020**, *137*, 48668.
[30] H. Lopez Hernandez, J. W. Souza, E. A. Appel, *Macromol. Biosci.* **2021**, *21*, e2000295.
[31] F. Zhou, Y. Hong, X. Zhang, L. Yang, J. Li, D. Jiang, V. Bunpetch, Y. Hu, H. Ouyang, S. Zhang, *Appl. Mater. Today* **2018**, *13*, 32.
[32] J. H. Jeong, Y. Liang, M. Jang, C. Cha, C. Chu, H. Lee, W. Jung, J. W. Kim, S. A. Boppart, H. Kong, *Tissue Eng Part A* **2013**, *19*, 1275.
[33] J. Zhong, Y. Yang, L. Liao, C. Zhang, *Biomater. Sci.* **2020**, *8*, 2734.
[34] W. J. Hadden, J. L. Young, A. W. Holle, M. L. McFetridge, D. Y. Kim, P. Wijesinghe, H. Taylor-Weiner, J. H. Wen, A. R. Lee, K. Bieback, B.-N. Vo, D. D. Sampson, B. F. Kennedy, J. P. Spatz, A. J. Engler, Y. S. Choi, *Proc. Nat. Academy Sci.* **2017**, *114*, 5647.
[35] B. Yang, K. Wei, C. Loebel, K. Zhang, Q. Feng, R. Li, S. H. D. Wong, X. Xu, C. Lau, X. Chen, P. Zhao, C. Yin, J. A. Burdick, Y. Wang, L. Bian, *Nat. Commun.* **2021**, *12*, 3514.
[36] S. Sankaran, E. Cavatorta, J. Huskens, P. Jonkheijm, *Langmuir* **2017**, *33*, 8813.
[37] Q. An, J. Brinkmann, J. Huskens, S. Krabbenborg, J. de Boer, P. Jonkheijm, *Angewandte Chem. Int. Ed.* **2012**, *51*, 12233.

SUPPORTING INFORMATION

Additional supporting information may be found in the online version of the article at the publisher's website.

How to cite this article: A. A. Aldana, F. L. C. Morgan, S. Houben, L. M. Pitet, L. Moroni, M. B. Baker, *J. Polym. Sci.* **2021**, *59*(22), 2830. https://doi.org/10.1002/pol.20210554